Stability and electronic properties of hybrid SnO bilayers: SnO/graphene and SnO/BN

Qing Guo[1], Gaoxue Wang[1], Ashok Kumar[2] and Ravindra Pandey[1]

[1]Department of Physics, Michigan Technological University, Houghton, Michigan 49931, USA
[2]Centre for Physical Sciences, Central University of Punjab, Bathinda, Punjab 151001, India

(Sep 27, 2017)

*Email: pandey@mtu.edu

Abstract

Van der Waals structures based on two dimensional materials have been considered as promising materials for novel nanoscale electronic devices. Two dimensional SnO films which display intrinsic p-type semiconducting properties were fabricated recently. In this paper, we consider the vertically stacked heterostructures consisting of SnO monolayer with graphene or BN monolayer to investigate their stability, electronic and transport properties using density functional theory. The calculated results find that the properties of the constituent monolayers are retained in these SnO-based heterostructures, and a p-type Schottky barrier is formed in the SnO/graphene heterostructure. Additionally, the Schottky barrier can be effectively controlled with an external electric field, which is useful characteristics for the van der Waals heterostructure-based electronic devices. In the SnO/BN heterostructure, the electronic properties of SnO are least affected by the insulating monolayer suggesting the BN monolayer to be an ideal substrate for the SnO-based nanoscale devices.

1.0 Introduction

Two-dimensional (2D) materials exhibit novel nanoscale properties for the next-generation electronic devices. Additionally, structures consisted of two or more 2D materials interacting via the van der Waals (vdW) forces provide a unique way of fabricating heterojunctions which can be used as building blocks in a variety of nanoscale devices [1]. For example, the phosphorene/graphene heterostructure displays tuning of the contact from n-type Schottky to p-type Schottky and then Ohmic by simply tailoring the relative position of the graphene's Fermi level within the phosphorene's band gap [2]. Additional examples of such heterostructures include semiconducting transition metal dichalcogenides and graphene which are proposed for large-scale 2D electronics [3-9]. Note that synthesis and characterization of such heterostructures involving graphene is of particular interest due to graphene being material with a high electron mobility [10].

Tin monoxide (SnO), unlike most other oxide semiconductors, shows intrinsic p-type semiconductor characters due to the unintentional Sn vacancy presence[11, 12]. Bulk SnO has tetragonal PbO layered structure with the space group of *P*4/*nmm*. In the corresponding single layer structure, oxygen atoms are at the middle plane, while each Sn atom forms a pyramid structure with the four neighboring O atoms. These pyramids alternatively distribute on both sides of the SnO layered structure (Supplementary Information, Figure S1). The properties like intrinsic p-type conduction and a large optical bandgap have generated significant interest in this novel 2D material [11, 13-20]. For example, this material can be used to produce high performance p-channel thin-film transistors (TFTs) [14]; double layers of SnO under suitable strain could be promising catalyst for photocatalytic water splitting[16]; its monolayer's multiferroic properties can be controlled by hole density [17]; and SnO sheets can be promising materials for sodium ion battery (SIB) applications [18]. In the multilayered SnO films with intrinsic p-type semiconducting properties, the direct optical band gap is measured to vary from 3.53 eV to 2.80 eV in going from 2-layers to 9-layers in thickness [19]. The band gap of the bulk-like film is 2.95 eV [16]. Recently, the p-n heterojunctions consisting of SnO and MoS_2 layers has been successfully fabricated [21].

In this paper, we now investigate a feasibility of forming 2D heterostructures of SnO/graphene or SnO/BN monolayer focusing on their stability and electronic properties. Specifically, we will ask the questions: Can a SnO monolayer form a vdW heterostructure with graphene or BN monolayer? If such a

heterostructure is stable, can it display characteristics of a typical *p-n* type heterojunctions under the application of an external electric field? Employing density functional theory, we will first calculate properties of monolayer and bilayers of SnO to establish a reference point for SnO heterostructures formed with graphene or BN monolayer. Next, the structural stability and electronic properties of SnO/graphene and SnO/BN heterostructures will be determined. Finally, the effect of external electric field applied perpendicular to the heterostructure will be investigated to ascertain the properties of the heterojunctions formed by the constituent monolayers.

2.0 Computational methods

Electronic structure calculations were carried out within the framework of the density functional theory (DFT) by using the Vienna ab-initio Simulation Package (VASP) program [22, 23]. The generalized-gradient approximation (GGA) proposed by Perdew-Burk-Ernzerhof (PBE) [24] together with Grimme's D2 method [25] representing the van der Waals interaction term were employed. The energy convergence was set to 10^{-7} eV and the kinetic energy cut-off was 520 eV. The geometry optimization was considered to be converged when the residual force on each atom was smaller than 0.01 eV/Å. The reciprocal space was sampled by a grid of (13x7x1) k points for the structural optimization calculations. A larger (33x17x1) k-point grid was used for calculations of electronic properties including density of states (DOS) and band structure. In the periodic supercell calculations of heterostructures, the vacuum distance normal to the plane was larger than 14 Å to eliminate the interaction between the replicas.

To test the reliability of our modeling elements, we first performed calculations on the bulk SnO. The calculated structural parameters for the bulk SnO agree very well with the corresponding experimental [19, 26] and the previously reported theoretical studies [12, 27-31] (Supplementary Information, Table S1). For example, the calculated lattice constants, *a* and *c* are 3.835 Å and 4.817 Å, respectively, as compared to the corresponding experimental values 3.801 Å and 4.835 Å for the bulk SnO. The calculated interlayer distance is 2.68 Å. We find that the inclusion of vdW interactions via the D2 term in calculations appear to be important for the bulk SnO as it increases the interlayer binding energy from 0.15 eV to 0.73 eV per SnO unit cell, and yields a more accurate interlayer distance of 2.48 Å as compared to the

experimental value of 2.52 Å.

3.0 Results and discussions

3.1 Equilibrium configuration and stability

To find the energetically preferred stacking configurations for heterostructures, the registry index (RI) model was initially used. The RI model employs simple geometric considerations to obtain energetically preferred configurations of a multilayer system with the modest computational resources [32]. The stability defined by the binding energy obtained from the RI index which, in turn, is proportional to the projected overlap area between the adjacent atoms at the interface of the heterostructure (Supplementary Information, Figures S2 and S3). The RI configurations for the SnO-based heterostructures are then taken as initial configurations for the DFT calculations. Following the stacking nomenclature of graphite, we define the stacking configurations to be AA (i.e. one of the bottom Sn atoms is on top of a C atom of graphene) and AB (i.e. one of the bottom Sn atoms is located over the hollow site of the hexagonal lattice) as displayed in Figure 1.

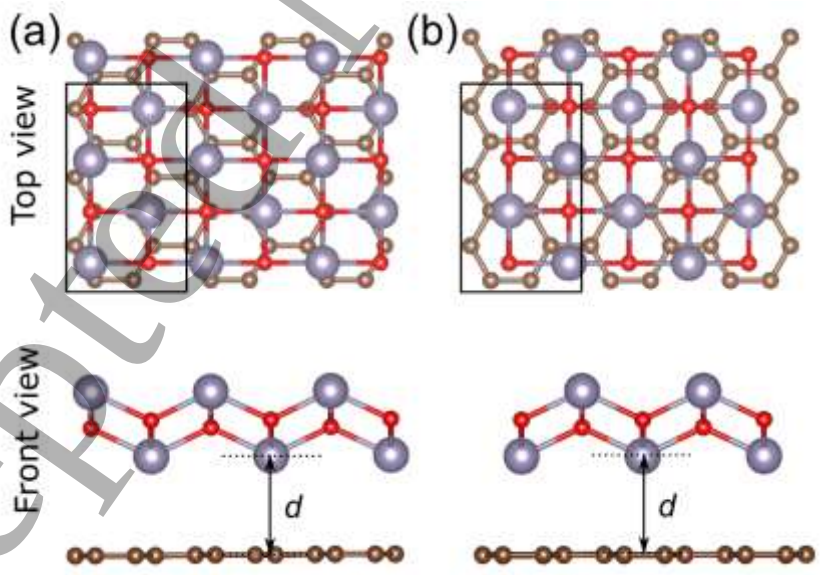

Figure 1: A schematic diagram of the (a) AA- and (b) AB-stacking configurations of the SnO/Graphene heterostructure. The red, grey and brown balls represent O, Sn and C atoms, respectively.

For the SnO/graphene heterostructure, the DFT results find the AB-stacked configuration to be preferred with the binding energy of 0.24 eV/SnO unit cell and the interlayer distance of 3.42 Å. The bond distances R_{Sn-O} and R_{C-C} are 2.35 (2.24) and 1.42 (1.41) Å in x (y) direction, respectively. The AA-stacked configuration is slightly higher in energy with the binding energy of 0.23 eV/SnO unit cell and the interlayer distance of 3.47 Å. Replacement of graphene with the BN monolayer in the heterostructure also yields the AB-stacked configuration to be energetically preferred with the binding energy of 0.29 eV/SnO unit cell and the interlayer distance of 3.36 Å. Note that calculations for the SnO bilayer find the AA-stacked configuration to be energetically preferred with the interlayer distance of 2.50 Å and the binding energy of 0.35 eV/unit cell (Supplementary Information, Figure S4, and Table S2), which follows the structure of bulk SnO. The calculated lattice constant is 3.84 Å with the R_{Sn-O} bond distance of 2.25 Å for the SnO bilayer.

3.2 **Electronic properties**

For the SnO/graphene heterostructure, the calculated band structure and density of states (DOS) are displayed in Figure 2. The band structure of the heterostructure shows features of the constituent monolayers including Dirac-cone points of graphene (red dots), and direct/indirect band gaps of the SnO monolayer. A small band gap of about 8 meV is opened up in graphene suggesting a small but noticeable degree of the interlayer coupling in the heterostructure.

The band alignments of graphene, BN, SnO and the corresponding heterostructures are summarized in Figure 3. Overall, the band alignments in the heterostructures are comparable to the constituent monolayers indicating the presence of the weak vdW interactions between monolayers in the heterostructure. Interestingly, we notice that a Schottky barrier is formed in the heterostructure of SnO and graphene. According to the Schottky–Mott model at the interface between a metal and a semiconductor, the Schottky barrier is defined as the energy difference between the Fermi level of the metal and the conduction band minimum (CBM) or valence band maximum (VBM) of the semiconductor. If the Fermi level of metal is closer to the CBM, n-type Schottky barrier is formed. Otherwise, p-type Schottky barrier is formed.

In the case of SnO/graphene heterostructure, the Fermi level of graphene is closer to VBM of the SnO monolayer (Figure 2) that results into a p-type Schottky barrier with a height of 0.41 eV as illustrated in Figure 3(a). Additional calculations were also performed to illustrate the change in Schottky barrier height with the increasing thickness of the oxide layer. The results find that the Schottky barrier height decreases from 0.41 eV for SnO monolayer to 0.10 eV for SnO bilayer and 0.11 eV for SnO trilayer in the SnO-based heterostructures (Supplementary Information, Figure S6). For the SnO/BN heterostructure, the band structure and values of band energies (Figure 3(b), Supplementary Information, Figure S7) of the SnO monolayer have not been modified by the BN monolayer, implying that the insulating BN monolayer can be an ideal substrate for the SnO based electronic devices.

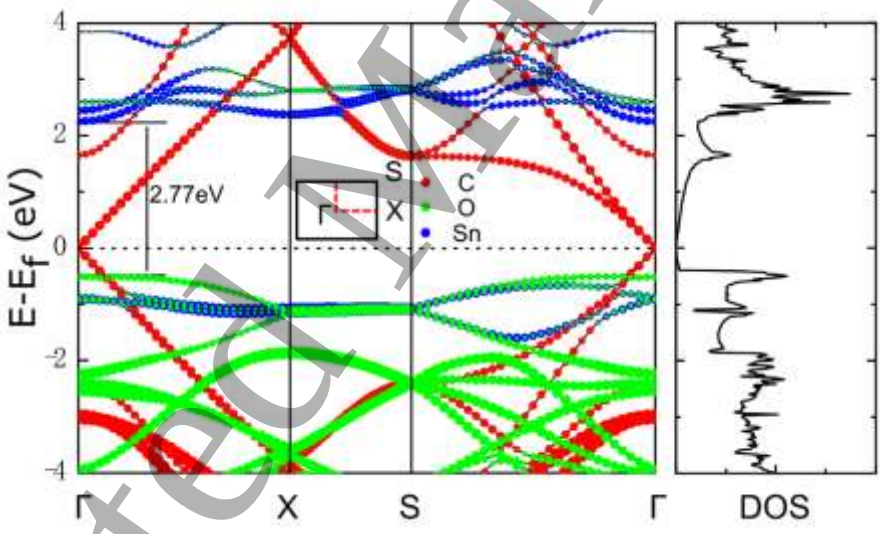

Figure 2. SnO/graphene heterostructure: Calculated band structure and total density of states. The bands projected to C, Sn and O atoms are displayed by red, blue and green dots respectively.

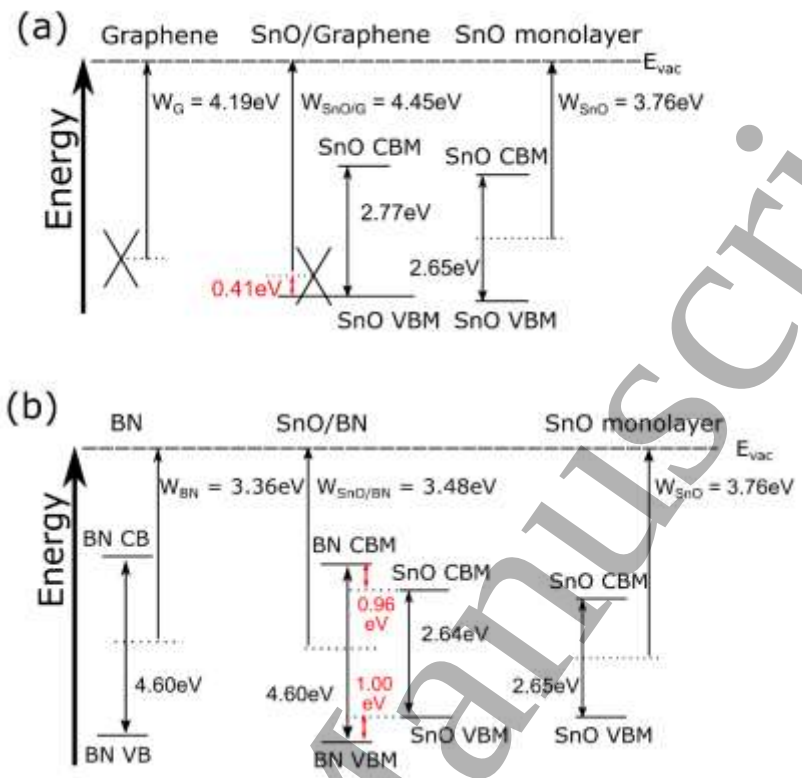

Figure 3. (a) Band alignments of graphene, SnO monolayer and SnO/graphene bilayer with respect to the vacuum level. (b) Band alignments of energy levels of graphene, SnO monolayer and SnO/BN bilayer with respect to the vacuum level. The black cone represents the Dirac point of graphene. SnO-VBM and SnO-CBM are valence band and conduction band edges of SnO with respect to the vacuum level, respectively. WG, W_{SnO}, $W_{SnO/G}$ and $W_{SnO/BN}$ are work functions of graphene, SnO monolayer, SnO/graphene and SnO/BN, respectively.

In the heterostructure, an unambiguous signature of the interlayer coupling can be seen in the charge density difference plots displayed in Figure 4. The electron localization function (ELF) plot (Figure 4(c)) shows an asymmetric ELF sphere further suggesting existence of the interfacial interaction in the heterostructure. The ELF sphere is associated with the lone pair of a Sn atom formed due to coupling between Sn ($5p_z$) orbital and the anti-bonding Sn (5s)–O ($2p_z$) hybridized orbitals (Supplementary Information, Figure S9) [12].

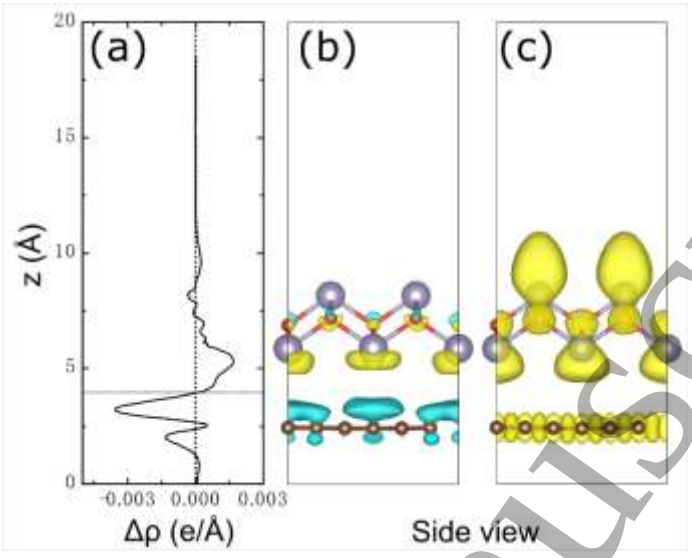

Figure 4. (a) The profile of the planar average charge density difference as a function of position along the z direction. The horizontal dashed line denotes the central location between SnO layer and graphene. (b) A side view of the charge density difference with the isosurface value of 0.0002 e/Å^3. (The yellow and blue colors represent electron-rich and electron-deficient regions, respectively.) (c) Electron localization function (ELF) of the SnO/graphene heterostructure with the isosurface value of 0.8.

To affirm the cause of opening of the band gap in graphene due to the presence of the oxide monolayer, we performed calculations with a shorter interlayer spacing of 2.62 Å to mimic the strengthening of the interaction between the individual monolayers in the heterostructure. This has resulted in a noticeable opening of the band gap of graphene to 27 meV without modifying broad features of the band structure of the heterostructure (Supplementary Information, Figure S5).

For the SnO/BN heterostructure, the constituent monolayers retain their individual features in the band structure. The minimum band gap of 2.6 eV is found to be associated with the SnO monolayer since the BN monolayer has a large band gap of 4.6 eV (Supplementary Information, Figure S7). Note that the structural property of the h-BN monolayer is similar to that of graphene.

It is to be noted that the DFT calculations for the SnO-based heterostructures were performed in the context of the 'commensurate lattice approximation' where graphene was used as a reference lattice. Initially, a (1×3) cell for graphene and a (1×2) cell for the SnO monolayer were used in the periodic supercell simulating the heterostructure. Due to lattice mismatch between the SnO monolayer and

graphene, the oxide monolayer is elongated in the *x*-direction and is shortened in the *y*-direction. The calculated lattice constant (*a =b)* of the pristine SnO monolayer is 3.81 Å, and the values of *a* and *b* for graphene are 4.26 Å and 2.46 Å, respectively.

To understand the effect of lattice mismatch in the heterostructure, a larger supercell consisting of a (7×3) cell for graphene and a (8×2) cell for the SnO monolayer was considered (Supplementary Information, Figure S8). We find that the structural properties are nearly converged; the interlayer distance is 3.42 Å (3.50 Å) and the binding energy value is 40 meV/C atom (41 meV/C atom) for the small (large) supercell. Likewise, we find a similarity in their band structures (Supplementary Information, Figure S8). In the following, we therefore present the results associated with the smaller supercell simulating the SnO/graphene heterostructure. Note that heterostructures with the noticeable lattice mismatch have been fabricated including phosphorene/graphene [2] and WSe_2/graphene [33].

3.3 Effect of external electric field

To consider the effect of a gate field on the electronic properties of a heterostructure in a device configuration, calculations in the presence of an external electric field were performed in which the forward direction of the electric field was taken from the oxide monolayer to graphene.

Figure 5 displays the calculated band structures in the presence of the electric field applied perpendicular to the heterostructure. The results show that application of the positive electric field shifts SnO-CBM to the lower values relative to the Dirac point (the red line in Figure 5(b)). On the other hand, SnO-VBM moves away from the Dirac point as shown by the blue line in Figure 5 (b). This movement of the band edges led to conversion of the *p*-type Schottky barrier to n-type with electric field at 0.7 eV/Å. When a negative electric field is applied, SnO-VBM touches the Fermi level with electric field larger than 0.5 eV/Å making the heterojunction to be Ohmic. Note that obtaining zero or even very low Schottky barrier in heterojunctions is very important for the realization of the high-performance field-effect transistors (FETs) [34]. Tuning of the contact type can therefore be achieved by the external electric field applied to the SnO/graphene heterostructure.

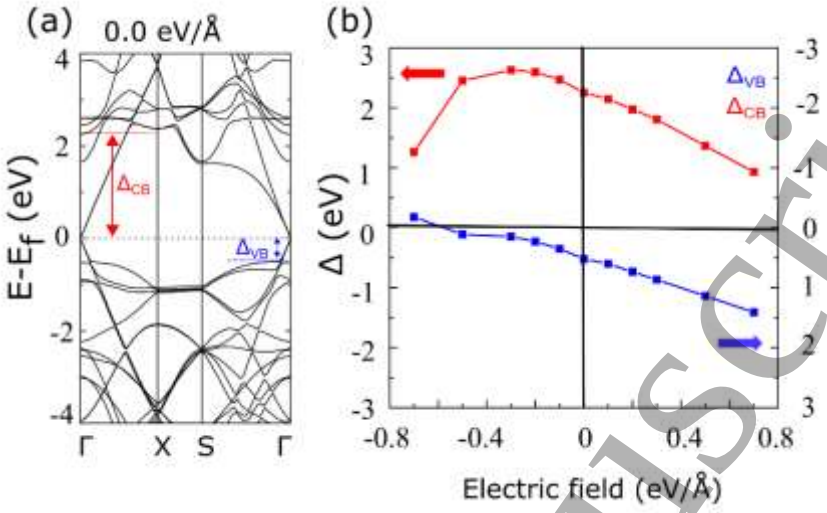

Figure. 5. SnO/graphene heterostructure: The band structures calculated for EF=0 eV/Å. (b) Variation of SnO-VBM (blue) and SnO-CBM (red) with applied electric field.

3.4 Electronic transport properties: Calculations of tunneling currents

Next, we use a conventional setup mimicking the scanning tunneling microscope (STM) experiments to calculate the tunneling current from the sample to the tip at location $\vec{r}_t$ based on Tersoff and Hamann approximation [35] :

$$I(\vec{r}_t;V) \approx \frac{2\pi e}{\hbar}\int_{-\infty}^{+\infty}\rho_t\left(E-\frac{eV}{2}\right)\rho_s\left(\vec{r}_t;E+\frac{eV}{2}\right)F(E)dE \qquad (1)$$

where ρ_t is the electron density of the tip, ρ_s is the electron density of the sample at the location of the tip. $F(E)$ is the term to include the effect of thermally excited electrons as proposed by He *et al*. [36]. This approach has been successfully used to investigate tunneling characteristics of several nanomaterials including PbS quantum dot, MoS_2 and BN monolayers, and phosphorene by our group [37-39]. The cap of the tip used in the STM measurements was simulated by Au_{13} cluster in our calculations.

The calculated tunneling currents associated with the heterostructures together with that of the oxide monolayer are plotted in Figure 6 over the range of external bias between -1.5 V and +1.5 V. It is important to note that the tunneling current is an integration of the convolution of DOS of the tip and the sample, and will depend on the filled and unfilled electron states near the Fermi energy of a given system.

Also, the magnitude of the current will depend on the tip-monolayer distance which will not, however, influence the trends in the I-V characteristics predicted in Figure 6.

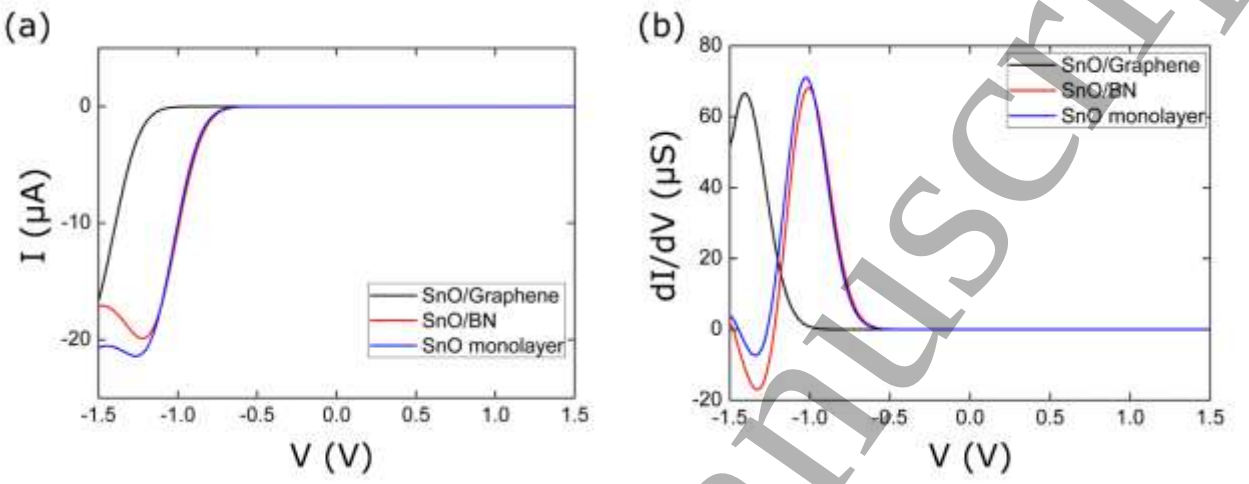

Figure. 6: (a) The current-voltage characteristics and (b) the calculated differential conductance curve of SnO monolayer, SnO/graphene and SnO/BN heterostructures.

For the pristine SnO monolayer, the threshold voltage is about -0.5 V and thereafter an approximately linear relationship of the tunneling current vs. voltage is seen. This is also the case with the heterostructures, though the threshold voltage of SnO/graphene (≈ -0.9 V) is slightly higher than that of the SnO/BN heterostructure (≈ -0.5 V). The presence of BN monolayer does not modify the I-V characteristics of the SnO monolayer, however, a clear shift toward negative bias is predicted for SnO/graphene due to the change of its Fermi level. Figure 6 (a) also displays the negative differential resistance (NDR) effect at about -1.3 V for the SnO monolayer and the SnO/BN heterostructure as also confirmed by differential conductance curves shown in Figure 6 (b). This small, but noticeable NDR effect appears to be associated with an overlap of the density of states of tip and SnO in these heterostructures (Supplementary Information, Figure S10).

To characterize topography of the SnO-based heterostructures, we now show the simulated STM images generated from the position-projected tunneling currents (Figure. 7). In simulations, we have used the constant current mode with the tip moving over the surface. The STM images show similar

characteristics with the bright regions forming a rectangular pattern which is consistent with the geometrical configuration of SnO monolayer. Note that the bright regions correspond to the top-most Sn atoms in the heterostructures.

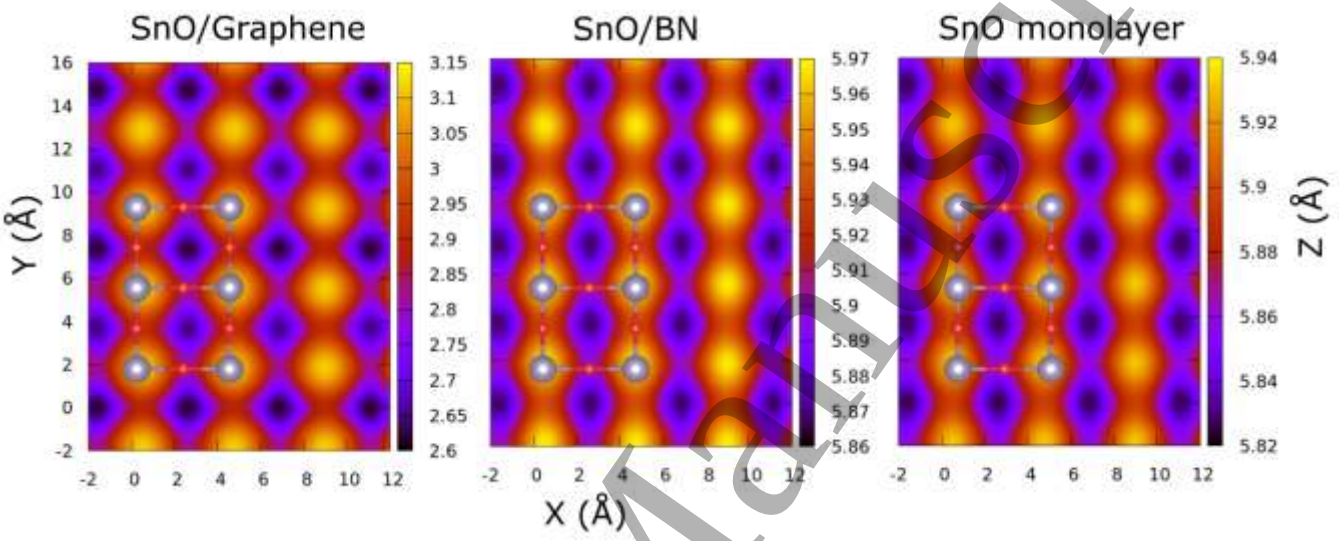

Figure 7. The STM images at constant current (0.3 nA, 1V) of (a) SnO/graphene. (b) SnO/BN heterostructures and (c) SnO monolayer.

In 2D materials, it is generally known that the excitonic effect is important due to the anti-screening effect and the relatively large effective mass. Calculation were performed using the HSE functional form [40] which finds the band gap to be 3.7 eV for the monolayer. Following the work of Jiang et al. [41] one can then approximate the exciton binding energy to be 0.93 eV. Note that a linear scaling law between the quasiparticle band gap and the exciton binding energy for two dimensional materials has previously been suggested. [41]

There exists a possibility of fabricating the SnO-based heterostructures since the graphene heterostructures with phosphorene [2] and WSe_2 [33] have been fabricated for which the calculated binding energy values are 60 and 54 meV/C atom, respectively. In the present case, the calculated binding energy of the SnO/graphene heterostructure is 40 meV/C atom. Also, the vdW 2D heterostructures consisted of graphene and MoS_2 monolayers have been fabricated, though there exists a lattice mismatch

between graphene and MoS_2. The lattice constants of MoS_2 and graphene are 3.15 and 2.46 Å, respectively[21].

4.0 Summary

In summary, we have investigated the structure and electronic properties of the SnO/graphene and SnO/BN heterostructures by using density functional theory. We show that the electronic properties of the SnO monolayer are preserved when it is placed on the top of graphene or BN monolayer. In the heterostructures, external electric field can manipulate the SnO monolayer band structure relative to the graphene's Dirac point, and turn this *p*-type junction into n-type with positive bias and to Ohmic contact with negative bias.

Acknowledgements

Helpful discussion with Kevin Waters and Max Seel are acknowledged. RAMA and Superior, high performance computing clusters at Michigan Technological University, were used in obtaining results presented in this paper. Supports from Dr. S. Gowtham are gratefully acknowledged.

References

1. Geim, A.K. and I.V. Grigorieva, *Van der Waals heterostructures.* Nature, 2013. **499**(7459): p. 419-25.
2. Padilha, J.E., A. Fazzio, and A.J. da Silva, *Van der Waals heterostructure of phosphorene and graphene: tuning the Schottky barrier and doping by electrostatic gating.* Phys Rev Lett, 2015. **114**(6): p. 066803.
3. Pierucci, D., et al., *Band Alignment and Minigaps in Monolayer MoS2-Graphene van der Waals Heterostructures.* Nano Lett, 2016. **16**(7): p. 4054-61.
4. Yu, L., et al., *Graphene/MoS2 hybrid technology for large-scale two-dimensional electronics.* Nano Lett, 2014. **14**(6): p. 3055-63.
5. Roy, K., et al., *Graphene-MoS2 hybrid structures for multifunctional photoresponsive memory devices.* Nat Nanotechnol, 2013. **8**(11): p. 826-30.
6. Kwak, J.Y., et al., *Long wavelength optical response of graphene-MoS2 heterojunction.* Applied Physics Letters, 2016. **108**(9): p. 091108.
7. Pandey, T., et al., *Pressure-Induced Charge Transfer Doping of Monolayer Graphene/MoS2 Heterostructure.* Small, 2016. **12**(30): p. 4063-9.
8. Britnell, L., et al., *Strong light-matter interactions in heterostructures of atomically thin films.* Science, 2013. **340**(6138): p. 1311-1314.
9. Xu, L.H., Wei-Qing; Hu, Wangyu; Zhou, Bing-Xin; Pan, Anlian; Huang, Gui-Fang, *2D MoS2-Graphene-based multilayer van der Waals heterostructures: Enhanced charge transfer and optical absorption, and electric-field tunable Dirac point and band gap.* {ArXiv e-prints}, 2016.
10. Novoselov, K.S., et al., *Electric field effect in atomically thin carbon films.* science, 2004. **306**(5696): p. 666-669.
11. Togo, A., et al., *First-principles calculations of native defects in tin monoxide.* Physical Review B, 2006. **74**(19).
12. Walsh, A. and G.W. Watson, *Electronic structures of rocksalt, litharge, and herzenbergite SnO by density functional theory.* Physical Review B, 2004. **70**(23).
13. Hosono, H., et al., *Bipolar conduction in SnO thin films.* Electrochemical and Solid-State Letters, 2011. **14**(1): p. H13-H16.
14. Ogo, Y., et al., *p-channel thin-film transistor using p-type oxide semiconductor, SnO.* Applied Physics Letters, 2008. **93**(3): p. 032113.
15. Ogo, Y., et al., *Tin monoxide as an s-orbital-based p-type oxide semiconductor: Electronic structures and TFT application.* physica status solidi (a), 2009. **206**(9): p. 2187-2191.
16. Zhou, W. and N. Umezawa, *Band gap engineering of bulk and nanosheet SnO: an insight into the interlayer Sn-Sn lone pair interactions.* Phys Chem Chem Phys, 2015. **17**(27): p. 17816-20.
17. Seixas, L., et al., *Multiferroic Two-Dimensional Materials.* Phys Rev Lett, 2016. **116**(20): p. 206803.
18. Zhang, F., et al., *Two-Dimensional SnO Anodes with a Tunable Number of Atomic Layers for Sodium Ion Batteries.* Nano Lett, 2017. **17**(2): p. 1302-1311.
19. Saji, K.J., et al., *2D Tin Monoxide-An Unexplored p-Type van der Waals Semiconductor: Material Characteristics and Field Effect Transistors.* Advanced Electronic Materials, 2016. **2**(4): p. 1500453.
20. Wang, Z., et al., *Hybrid van der Waals p-n Heterojunctions based on SnO and 2D MoS2.* Adv Mater, 2016. **28**(41): p. 9133-9141.
21. Wang, Z., et al., *Hybrid van der Waals p-n Heterojunctions based on SnO and 2D MoS2.* Adv Mater, 2016.

22. Kresse, G. and J. Furthmüller, *Efficient iterative schemes for \textit{ab initio} total-energy calculations using a plane-wave basis set.* Physical Review B, 1996. **54**(16): p. 11169-11186.
23. Kresse, G. and J. Furthmüller, *Efficiency of ab-initio total energy calculations for metals and semiconductors using a plane-wave basis set.* Computational Materials Science, 1996. **6**(1): p. 15-50.
24. Perdew, J.P., K. Burke, and M. Ernzerhof, *Generalized Gradient Approximation Made Simple.* Physical Review Letters, 1996. **77**(18): p. 3865-3868.
25. Grimme, S., *Semiempirical GGA-type density functional constructed with a long-range dispersion correction.* J Comput Chem, 2006. **27**(15): p. 1787-99.
26. Moreno, M.S. and R.C. Mercader, *Mössbauer study of SnO lattice dynamics.* Physical Review B, 1994. **50**(14): p. 9875-9881.
27. Meyer, M., et al., *Electronic structure of stannous oxide.* Computational materials science, 1998. **10**(1-4): p. 319-324.
28. Christensen, N., A. Svane, and E.P. y Blancá, *Electronic and structural properties of SnO under pressure.* Physical Review B, 2005. **72**(1): p. 014109.
29. McLeod, J., et al., *Nature of the electronic states involved in the chemical bonding and superconductivity at high pressure in SnO.* JETP letters, 2011. **94**(2): p. 142-146.
30. Govaerts, K., et al., *van der Waals bonding and the quasiparticle band structure of SnO from first principles.* Physical Review B, 2013. **87**(23): p. 235210.
31. Chen, P.-J. and H.-T. Jeng, *Phase diagram of the layered oxide SnO: GW and electron-phonon studies.* Scientific reports, 2015. **5**.
32. Hod, O., *Interlayer commensurability and superlubricity in rigid layered materials.* Physical Review B, 2012. **86**(7).
33. Yu, Z.G., Y.-W. Zhang, and B.I. Yakobson, *Strain-Robust and Electric Field Tunable Band Alignments in van der Waals WSe2–Graphene Heterojunctions.* The Journal of Physical Chemistry C, 2016. **120**(39): p. 22702-22709.
34. Kwon, J., et al., *Thickness-dependent Schottky barrier height of MoS2 field-effect transistors.* Nanoscale, 2017. **9**(18): p. 6151-6157.
35. Tersoff, J. and D.R. Hamann, *Theory and Application for the Scanning Tunneling Microscope.* Physical Review Letters, 1983. **50**(25): p. 1998-2001.
36. He, H., et al., *Spin-polarized electron transport of a self-assembled organic monolayer on a Ni(111) substrate: An organic spin switch.* Physical Review B, 2006. **73**(19): p. 195311.
37. Loh, G., et al., *MoS2 Quantum Dot: Effects of Passivation, Additional Layer, and h-BN Substrate on Its Stability and Electronic Properties.* The Journal of Physical Chemistry C, 2015. **119**(3): p. 1565-1574.
38. Wang, G., R. Pandey, and S.P. Karna, *Phosphorene oxide: stability and electronic properties of a novel two-dimensional material.* Nanoscale, 2015. **7**(2): p. 524-531.
39. Gupta, S.K., et al., *Electron tunneling characteristics of a cubic quantum dot,(PbS) 32.* The Journal of chemical physics, 2013. **139**(24): p. 244307.
40. Krukau, A.V., et al., *Influence of the exchange screening parameter on the performance of screened hybrid functionals.* J Chem Phys, 2006. **125**(22): p. 224106.
41. Jiang, Z., et al., *Scaling Universality between Band Gap and Exciton Binding Energy of Two-Dimensional Semiconductors.* Phys Rev Lett, 2017. **118**(26): p. 266401.